Effects of mass wasting on fluvial sediments in Puerto Rico following Hurricane Maria

Webb, N.D.S. [a]; Regmi, N. R. [b]; Soreghan, G.S. [a]; Elwood Madden, A.S. [a]; Sylvester, J. [a]; Cartagena Colon, F.; Demirel-Floyd, C. [a]; Elwood Madden, M.E. [a]

[a] School of Geosciences, The University of Oklahoma, Norman OK

[b] Oklahoma Geological Survey, The University of Oklahoma

Abstract

Mass wasting plays an important role on carbon cycling and sequestration by exposing fresh, weatherable bedrock and delivering hillslope sediments to lowlands and fluvial systems. Chemical weathering signatures of landslide-derived fluvial sediments can be used to understand linkages between hillslope and fluvial processes, and thus to characterize spatiotemporal dynamics of sediments. However, chemical signatures of fluvial sediments derived by landslides are yet to be fully understood. Here we compare the bulk chemistry, mineralogy, and grain size of fluvial sediments collected pre- and post-Hurricane Maria (landfall on Sept. 20, 2017) in the Rio Guayanés and Rio Guayabo River watersheds in southeastern Puerto Rico to help fill this knowledge gap.

Relative to fluvial muds collected before Hurricane Maria, mud samples collected after the storm exhibit higher weathering index values, but coarser grain size modes. We infer that small landslides triggered by Hurricane Maria transported slope materials from shallow depths, including weathered topsoil and saprolite, as opposed to previous deep-seated landslides which likely sampled regolith and bedrock. The variances in weathering indices observed pre- and post-hurricane do not reflect climate change, but rather subtle differences in transport mechanism which produce significant differences in weathering indices recorded by fluvial sediments. We propose that weathering indices provide a means to understand sediment dynamics in mountainous regions, particularly for sediment transported in the immediate aftermath of landslides triggered by extreme events, such as precipitation and earthquakes, and also provide important datasets required for mapping potential carbon sequestration across a landscape.

Keywords: Mass Wasting, Chemical Index of Weathering, Hurricane Maria, Fluvial Sediments, Carbon Sequestration

1. Introduction

Physiochemical characteristics of fluvial sediments have the potential to inform complex linkages among climatic, tectonic, hillslope and geomorphic processes. For example, weathering trends in fluvial sediments can shed light on rates and frequency of sediment production and transport from upland hillslopes, and thus provide a potential signature of both short- and long-term sediment transport and carbon cycling as well as a paleoclimate (White et al., 1998; White, Bullen, Vivit, Schulz, & Clow, 1999). Mass wasting is one of the major processes that deliver hillslope materials to fluvial systems in moderate - to high - relief settings. Increased mass wasting owing to climate and land-use change may increase chemical weathering rates (Moore, Buss, & Dosseto, 2019; Oliva, Viers, & Dupré, 2003), resulting in consumption of atmospheric carbon dioxide and producing a negative feedback effect for global climate change over thousands to millions of years, as well as immediately affecting stream quality and ecology (Sassa & Canuti, 2008).

Chemical weathering of fresh bedrock delivers cations into fluvial systems and draws down pCO_2 from Earth's atmosphere (Berner, 2003; Fernandes, da Conceição, Junior, de Souza Sardinha, & Mortatti, 2016). However, landslides may be a net source of CO_2 to the atmosphere where exposure of carbonates and sulfides result in sulfuric acid weathering of the carbonates (Emberson, Galy, & Hovius, 2018). Thus, the mineralogy of the weathering bedrock plays an important role in determining whether carbon is sequestered or released to the atmosphere.

The relative size and the frequency of the landslides also plays an important role in determining sediment volume, as well as degree of weathering, delivered to the fluvial system. For example, shallow landslides occur frequently and transport highly weathered soil and/or saprolite, whereas deep-seated landslides tend to occur less frequently, but transport large volumes of slope materials including soil, less-weathered saprolite, and deeper bedrock

(Bessette-Kirton et al., 2019; Stark & Hovius, 2001). Landslide size and frequency across a landscape is primarily governed by the spatial structure of hillslope strength variability (Bessette-Kirton et al., 2019; Varnes, 1978) which is influenced by: 1) hillslope morphology (i.e. slope, curvature, etc.) (Schmidt & Montgomery, 1995); 2) lithological characteristics, including the depth and bio-physiochemical properties of soil and underlying bedrock characteristics, including type, fracture density, and composition (Clarke & Burbank, 2011; Dixon, Heimsath, Kaste, & Amundson, 2009; Phillips, Marion, Luckow, & Adams, 2005); 3) associated surface and sub-surface hydrology; and 4) triggering mechanisms, such as precipitation, earthquakes, and anthropogenic activities (Lehmann et al., 2013; Varnes, 1978).

The impact of mass wasting on the weathering indices of sediment delivered to streams in high-relief and high-precipitation landscapes is not well known, and may provide important evidence of historical weathering trends, or could predict trends likely to occur with future mass-wasting (Bluth & Kump, 1994; Joo, Elwood Madden, & Soreghan, 2018). Mass wasting introduces a range of sediment grain sizes to fluvial systems (Larsen & Torres-Sanchez, 1998), which may also depend on several additional factors including 1) bedrock lithology (Roda-Boluda, D'Arcy, McDonald, & Whittaker, 2018), 2) rates of chemical weathering, particularly in tropical regions where more chemical weathering leads to finer grain sizes (Fernandes et al., 2016), and 3) transport mechanisms. For example, sediment supplied from gradual erosion of soil via overland flow tends to be finer grained and more homogeneous (i.e. well-sorted) (Attal et al., 2015), while sediment supplied via landslides tends to be coarser and poorly sorted, and can result in coarsening downstream, compared to the general trend of distal fining expected in a typical fluvial system (Attal et al., 2015; Roda-Boluda et al., 2018; Struck et al., 2015). In

addition, steep slopes in humid climates with abundant precipitation are more susceptible to mass wasting versus steep slopes in arid climates (Gariano & Guzzetti, 2016; Shiels & Walker, 2013).

Due to stochastic events, such as mass wasting, fluvial sediment properties can vary widely across both space and time. Anomalously low chemical index of alteration (CIA) values observed in fluvial sediments collected from the granitic watershed study area in Puerto Rico in 2014 were previously attributed to significant influence of mass wasting that tapped less-weathered regolith (Joo et al., 2018). Joo et al. (2018) posited that future climate warming and attendant increased precipitation might further stimulate delivery of mass-wasted material to streams, resulting in lower values of weathering indices in fluvial sediment. Hurricane Maria, which passed over Puerto Rico on September 20, 2017, resulted in >500 mm of rainfall within 48 hours (Silva-Tulla, Pando, Pradel, Park, & Kayen, 2020) and triggered widespread mass wasting in the study area (Bessette-Kirton et al., 2019; Keellings & Ayala, 2019; Ramos-Scharrón & Arima, 2019). This natural disaster caused enormous loss of life, health, and property (Bessette-Kirton et al., 2019; Keellings & Ayala, 2019; Chiara Lepore, Kamal, Shanahan, & Bras, 2012), but also created a natural experiment in which to directly observe the immediate impact of hurricane-induced mass wasting on fluvial sediments.

Joo et al. (2018) predict that mass wasting events supply the fluvial system with larger grains that are less weathered and derived from bedrock, regolith, or saprolite rather than soils. Additionally, they predicted that mass wasting would deliver not only larger grain sizes than systems without mass wasting events, but also a wider range of grain sizes, and less weathered grains with deep-seated landslides (Attal et al., 2015; Hubert & Filipov, 1989). However, the potential impact of transient hillslope responses to intense but short-duration precipitation events on fluvial sediments remains poorly constrained. This study aims to investigate the short-term

impact of a significant storm event - Hurricane Maria, and the resultant landslides on fluvial sediment properties as well as bridge the gap between these properties and chemical weathering indices to analyze potential impacts on climate change.

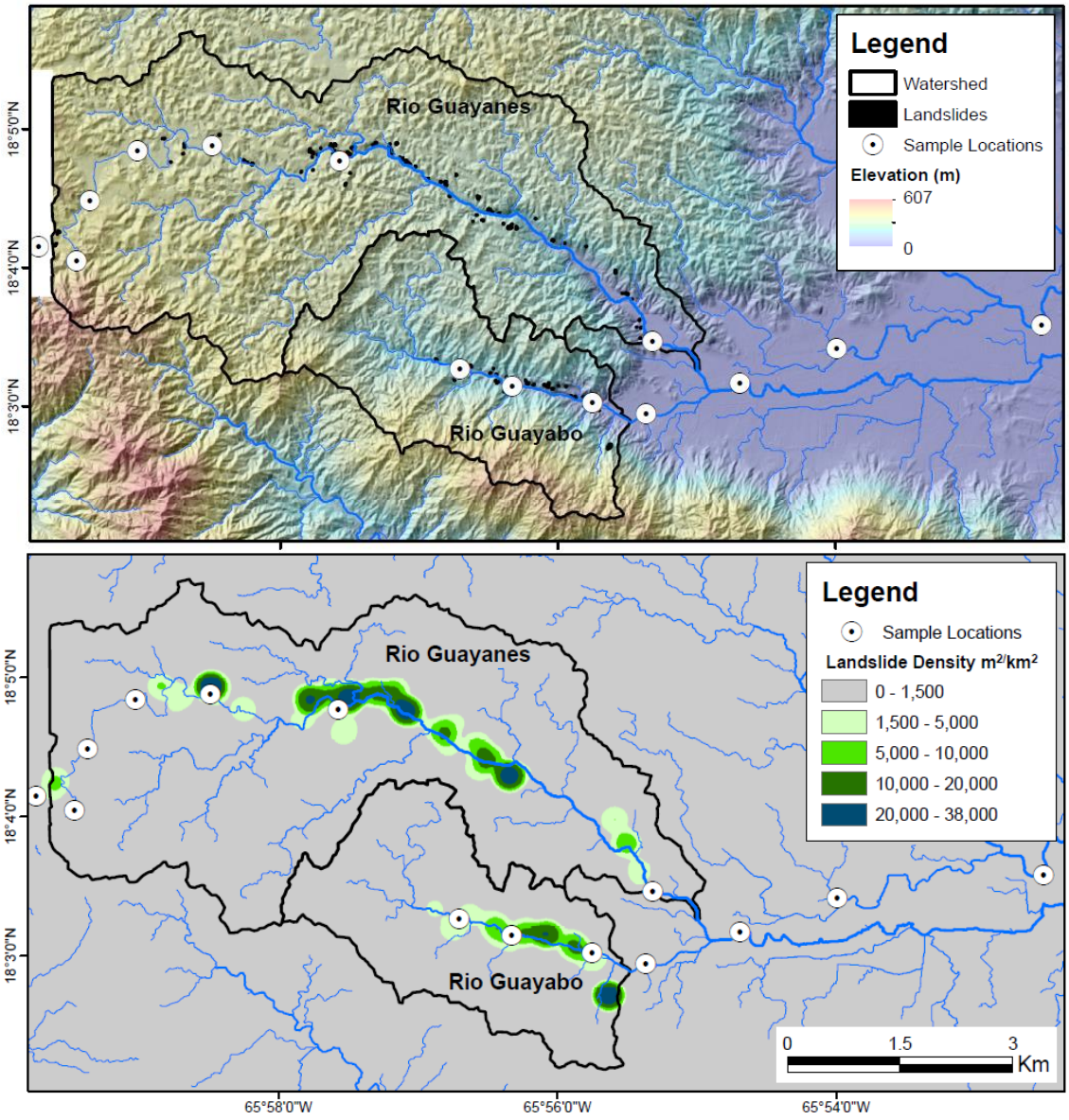

Figure 1: (A) Relief map of the Rio Guayanés located to the north and the Rio Guayabo in the south of the study region. Watersheds for the respective fluvial systems are outlined in black with sampling sites labeled as white circles and landslides indicated with black with arrows indicating landslides. (B) Inset map with study region highlighted by black box. Spatial density map for study region created using kernel density estimation of each of the mapped landslides within a 1 km^2 circular neighborhood.

2. Background

2.1 Geology

The regional tectonic system of Puerto Rico is characterized by left-lateral slip deformation along the Puerto Rico Trench, resulting in moderate earthquake activity (Masson & Scanlon, 1991). The specific study region is a part of the Cordillera Central Mountain range in southeastern Puerto Rico, which is characterized by Jurassic to Eocene igneous bedrock with a number of normal faults (Monroe, 1980). Major drainages in the study area include the Rio Guayabo and Rio Guayanés which also follow normal faults. The Rio Guayanés watershed is ~23 km^2 with a minimum elevation of 21 m and maximum elevation of 539 m above sea level. The Rio Guayabo watershed is ~8.5 km^2 with a minimum elevation of 23 m and maximum elevation of 497 m above sea level. Both fluvial systems are underlain by the Late Cretaceous San Lorenzo granodiorite (Rogers, Cram, Pease, & Tischler, 1977). In general, the granodiorite is overlain by ~2-8 m thick saprolite and ~0.5-1 m thick soil (Fletcher, Buss, & Brantley, 2006; Murphy, Stallard, Larsen, & Gould, 2012).

2.2 Climate and Land Usage

A tropical wet climate prevails, with an average annual temperature of ~25˚C, an average annual rainfall of ~768 mm, and approximately one hurricane every two years (Larsen, 2000; Chiara Lepore et al., 2012). Subtropical wet forests and sparsely populated rural areas prevail, where agricultural land use declined by ninety-five percent from 1951 to 2000 (Birdsey & Weaver, 1982; Martinuzzi, Gould, & González, 2007). During the 16th century, European settlers began massive deforestation to support agriculture, resulting in the destruction of the majority of mature forests by the 19th century (Birdsey & Weaver, 1982). Until the 1940s, sugar cane fueled the economy, driving near-total deforestation, with regional forest returning only since the 1950s

as a result of abandonment of small farms (Birdsey & Weaver, 1982). More recent anthropogenic activity in the form of road construction increases modern deforestation and destabilizes slopes; the highest density of landslides occur within close proximity to roads (Larsen & Parks, 1997).

2.3 Mass wasting

Landslides occur in mountainous terrains of Puerto Rico and cause loss of life and property (Bessette-Kirton et al., 2019; Keellings & Ayala, 2019; Chiara Lepore et al., 2012). Lepore et al. (2012) conducted a landslide susceptibility assessment of various areas in Puerto Rico and projected varying susceptibility attributable in part to the underlying bedrock lithology (Bessette-Kirton et al., 2019). The severe deforestation along with steep slopes and frequent high precipitation observed in Puerto Rico alone or in conjunction with seismic activity results in higher rates of erosion and mass wasting than in drier, less mountainous, or more forested terrains (Birdsey & Weaver, 1982).

2.4 Chemical weathering indices

Chemical weathering tends to be most intense in densely vegetated, tropical mountainous environments where surface and sub-surface hydrologic fluxes are high (Oliva et al., 2003). The chemical index of alteration, or CIA, is an indicator of the chemical weathering of feldspars to clays (Goldberg & Humayun, 2010). The CIA values of fluvial muds have been quantified for some tropical and subtropical areas and commonly used as a proxy for paleoclimate interpretations (Nesbitt & Young, 1982). The weathering of feldspars results in the removal of mobile cations such as calcium, potassium, and sodium which leads to an increase in the proportion of Al_2O_3 in the fluvial mud (Aristizábal, Roser, & Yokota, 2005; Nesbitt & Young, 1982). High CIA values (>90) are indicative of extensively weathered soil depleted in calcium

and sodium and enriched in aluminum (Nesbitt & Young, 1982). CIA values are calculated using the following equation developed by Nesbitt and Young (1982), where CaO* is silicate-bound.

$$Eq.1 \qquad CIA = \left[\frac{Al_2O_3}{(Al_2O_3 + CaO^* + Na_2O + K_2O)}\right] x\ 100$$

The CIA values observed in fluvial mud samples collected from the study area in 2014 were abnormally low (58-69) compared to expected values (>90), considering Puerto Rico exhibits very high weathering rates and a tropical-subtropical climate (Joo et al., 2018; White & Blum, 1995; White et al., 1998). Joo et al. (2018) noted that concentrations of CaO*, Na_2O, MgO, and Fe_2O_3 in the mud decreased distally, while K_2O increased distally, suggesting that the degree of chemical weathering observed in the sediments increases downstream, perhaps due to preferential transport of clays.

Ohta and Arai (2007) developed an alternative approach to determine both primary source lithology and weathering intensity (Ohta & Arai, 2007). This approach uses wt % SiO_2, TiO_2, Al_2O_3, Fe_2O_3, MgO, CaO, Na_2O, and K_2O in a multicomponent linear regression analysis to determine mafic (M) and felsic (F) portions of parent lithology and degree of weathering (W) of mafic and felsic portions, independent of the parent rock. Ternary plots of MFW have been used to display the multiple components, assuming normally distributed geochemical variability typically found in fresh mafic, fresh felsic, and weathered rock (Ohta & Arai, 2007). The combined utilization of different weathering indices based on the major elemental components of the lithology can help illustrate the extent of alteration based on the degree of elemental loss (Babechuk, Widdowson, & Kamber, 2014).

3. Methods

3.1 Landslide Mapping

We used aerial images archived in Google Earth and 1 m LiDAR topographic data (USGS National Map, 2020) to map post-Hurricane Maria landslides (24 September 2017 to 9 June 2018), and 10 m USGS National Elevation Datasets (NED) to map hillslope geometries and drainage network. Landslides were mapped only within a 350 m buffer of the Rio Guayanés and Rio Guayabo Rivers, based on our field observation that much of the sediment delivered to these streams appear to originate from landslides in adjacent hillslopes. The locations and characteristics of some of the landslides mapped from Google Earth and LiDAR shaded relief images were verified in the field. Landslide area was calculated in ArcGIS® and the volume of each landslide was modeled using an area (A) and volume (V) relationship ($V = 0.0254*A^{1.45}$) proposed by Regmi et al. (2014) for shallow landslides of the North Fork Gunnison River catchment of western Colorado. We apply this equation because of the similarity in geomorphic and lithological environments of this study with those of the North Fork Gunnison River catchment. In addition, the equation does not differ significantly from other area-volume relationships proposed for shallow landslides in various parts of the world (equations are listed in (Regmi et al., 2014; Tron, Dani, Laio, Preti, & Ridolfi, 2014)). However, some of the landslides mapped in this study are shallower than those documented in Regmi et al. (2014), suggesting the modeled volume and depths of some of the landslides in the Puerto Rico study may be slightly overestimated. The size (area, volume, and depth), frequency, and spatial density (Guzzetti et al., 2008) of observed landslides were then evaluated to explore if any relationship exists between spatial density and measured physiochemical characteristics of fluvial sediment.

3.2 Sediment and water sampling

Saprolite, fluvial sediment, and stream water samples were collected from the Rio Guayanés and Rio Guayabo in June 2018, nine months post-Hurricane Maria, using GPS

198 locations to ensure similar localities compared to Joo et al. (2018). Saprolite samples were
199 obtained from roadcut slopes (Figure 1). The top 2-5 cm of fine-grained sediment samples were
200 collected from the slack water areas of fluvial bars using a hand trowel at intervals ranging from
201 ~1-5 km between sampling locations, beginning at the upland source of the stream and
202 continuing ~21 km in total distance downstream (Figure 1). Sampling locations were determined
203 based on stream morphology and accessibility. Water samples were also collected from each of
204 these locations. Sediment and water samples were frozen upon returning to the lab and prior to
205 analyses.

206 3.3 Grain size, mineralogy, and surface area

207 All samples were wet sieved to obtain size fractions of gravel (>2 mm), sand (63 μm – 2
208 mm), and mud (<63 μm), then the mud was treated with buffered acetic acid and hydrogen
209 peroxide to remove carbonates (rare), and organic matter (abundant), respectively. The
210 remaining treated mud samples were freeze dried prior to specific surface area (SSA) analysis
211 using the six-point BET (Brunauer-Emmett-Teller) nitrogen adsorption isotherm (Brunauer,
212 Emmett, & Teller, 1938). The mud samples were passed through a 0.4 mm sieve to separate any
213 clumps to prepare the sample for a random mounting (Harris & Norman White, 2008) on a glass
214 slide for powder X-ray diffraction (XRD) analysis using the Rigaku Ultima IV diffractometer
215 using Cu-K-alpha radiation at 40 kV and 44 mA. We used the Bragg-Brentano method with a
216 range of 2-70° 2θ at 0.02° step size. Resulting diffraction patterns were analyzed with MDI
217 JADE Pro software and ICDD PDF-4+ database by whole pattern fitting for bulk mineral
218 identification.

219 3.4 Bulk geochemical analysis and chemical weathering indices

A split (~3-3.5 g) of the processed mud was sent to ALS Labs, where the solid samples were dissolved in strong acid and analyzed using inductively coupled plasma-atomic emission spectrometry (ICP-AES). In a few cases, the samples volumes were too small for analysis, so we added a known amount of corundum standard and later corrected for the added Al_2O_3 in the results.

The CIA values of the fluvial sediment mud fraction were then calculated using Equation 1, and the resulting data plotted on a ternary diagram of $CaO+Na_2O$, K_2O, and Al_2O_3 with more weathered samples plotting towards the Al_2O_3 vertex. Additionally, following Ohta and Arai (2007), an alternative chemical weathering index was also computed based on the bulk chemistry data that can be used to characterize mafic (M) and felsic (F) portion of rock source and degree of weathering (W) (Eq 1 in Supplementary Materials) and plotted on a MFW ternary diagram with more weathered samples plotting towards the W vertex.

3.5 Water chemistry

Water samples collected in the field were filtered through a 0.22 µm filter using a Millipore vacuum system, treated with 1 M hydrochloric acid and frozen. The samples were then sent to the Oklahoma State University Soil, Water and Forage Analytical Laboratory (http://soiltesting.okstate.edu/) where the samples were analyzed using inductively coupled plasma-optical emission spectrometry (ICP-OES). The resulting data were used to plot aqueous cation concentration versus distance downstream to analyze chemical weathering solutes released from the sediment within the fluvial system.

4. Results

4.1 Mass Wasting

Both field and aerial photographic mapping suggests that Hurricane Maria triggered mostly shallow landslides. We identified 116 shallow landslides that occurred within ~350 m from Rio Guayanés and Rio Guayabo during the nine-month period following Hurricane Maria (Figure 1). The area of these landslides ranges from ~11 m^2 to ~2,230 m^2 with an average area of ~238 m^2 (Table 1 and Figure 2a). Using the relationship in Regmi et al., (2014) the average volume is computed as ~110 m^3, and the average depth is computed as ~0.25 m with a standard deviation of 0.14 m (Table 1 and Figure 2b).

Table 1. Landslide area, volume* and depth*

Number of Landslides		116
Area (m^2)	Minimum	11
	Mean (airth.)	238
	Maximum	2230
Volume (m^3)	Minimum	1
	Mean (airth.)	110
	Maximum	1819
Depth (m)	Minimum	0
	Mean (airth.)	0
	Maximum	1

*Landslide volume was computed using the area-volume relationship proposed for western Colorado by (Regmi et al., 2014) and the depth was computed as a ratio of volume and area. Note: the average area (~238 m2) and volume (110 m3) may indicate that the average depth of the landslides is very shallow (~0.25 m). Full dataset in supplementary materials.

The landslide size-frequency plot (Figure 2) suggests that most of the observed landslides are relatively small. The landslides occur across a wide range of slope gradients with the largest frequency occurring at ~24-26˚, which also correlates to the most prevalent slopes in the area (Figure 2d). The average slopes of the entire landscape and areas containing landslides are 19.6 ˚

254 ± 9.3˚ and 19.7 ˚ ± 10.6 ˚, respectively. Similarly, the landslide spatial density map developed
255 using kernel density estimation and 1 km^2 circular neighborhood as a bandwidth shows the
256 highest density of landslides between samples five and seven along Rio Guayanés and between
257 three and four of the Rio Guayabo (Figure 1b).

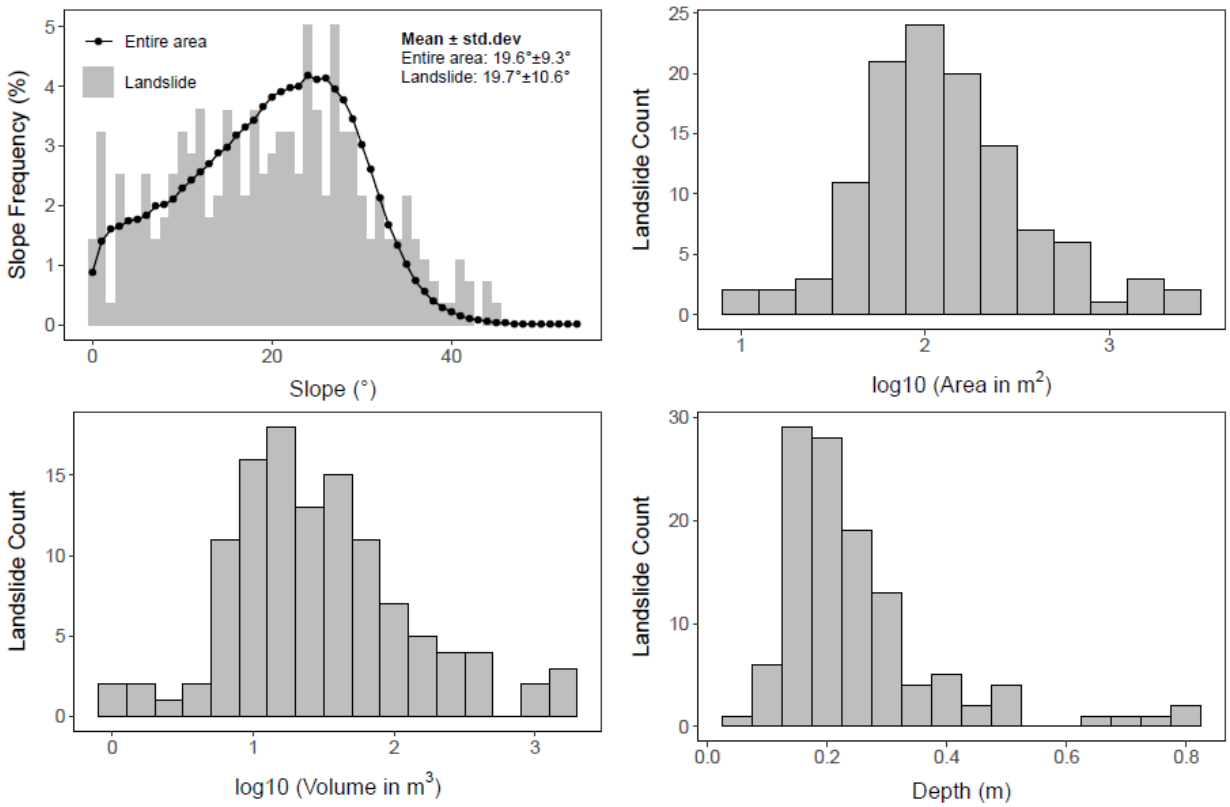

258

259 Figure 2: Observed hillslope characteristics including the distribution of slope gradients of
260 landslides and entire hillslopes (A), landslide area (B), modeled landslide volume (C), and
261 modeled average landslide depth (D). Note the landslide volume was computed using Landslide
262 area – volume relationship proposed by Regmi et al., 2014, and the depth was computed as a
263 ratio of volume and area.

264 4.2 Rio Guayanés Sediment

265 Overall, the sediment in the most proximal samples is coarser and displays more
266 variability in grain size distributions observed between different samples in 2018 compared to
267 2014 (samples 1-3). For samples collected in both 2014 and 2018, the weight percent of sand is
268 much higher (~75 wt%), than the weight percent of mud (<20 wt%) (Table 2 in Supplementary

Materials). However, the proportions of the sand and mud fractions display a wider range of variability in the post-hurricane 2018 sample set. The weight percent of mud is generally higher in samples collected in 2018 from the proximal and distal portions of the stream compared to the weight percent of mud in 2014 samples from the same locations (Table 2 in Supplementary Materials). The weight percent of gravel observed in the samples collected from the mid portion of the stream (samples 4-7) was much lower in 2018 than in 2014. The most distal samples (8-10), illustrate opposite weight percent trends in gravel from 2018 and 2014, with higher gravel concentrations observed distally in 2014.

The 2018 and 2014 sample sets exhibit opposing trends in weight percent of clay-sized grains along the stream course (Table 2 in Supplementary Materials): the 2018 samples show a higher proportion of clay-sized material in more proximal samples, whereas the 2014 samples display a higher proportion of clay-sized grains in distal samples. Changes in concentration of silt-sized grains are similar for both sampling years, but slightly higher in 2018. The modal grain size within the mud fraction also show opposing trends in the two sampling years, with the mud size modes increasing with distance downstream in 2018 and decreasing with distance downstream in 2014 (Table 2 in Supplementary Materials).

The mud size fraction collected in 2018 consists of mainly albite, quartz, amphibole, clay minerals, and mica (Table 3 in Supplementary Materials). No systematic change in mineralogy was observed from proximal to distal samples within the Rio Guayanés fluvial system in the 2018 samples, while the 2014 samples exhibited a general decrease of primary minerals (quartz, plagioclase, hornblende, and K-feldspar) in the distal samples (Joo et al., 2018).

The Rio Guayanés sediment CIA values indicate a higher degree of weathering in 2018. The mean CIA values of the 2018 sediment is ~80, ranging from 66-88, while the mean value

observed in the 2014 sediment is ~65, ranging from 58-69 (Figures 3 and 5). Similar to the CIA values, the Rio Guayanés sediment MFW values also indicate the 2018 sediment is more weathered when compared to 2014 samples (Figure 3) (Joo et al., 2018). As the surface area of sediment increases, CIA values are also expected to increase. Finer grained sediment fractions have a higher surface area available for weathering and are also more likely to contain clay minerals (White et al., 1996). This relationship is only slightly observed in the 2018 Rio Guayanés sediment, while this trend is strongly observed in the 2014 Rio Guayanés sediment samples (Table 4 in Supplementary Materials).

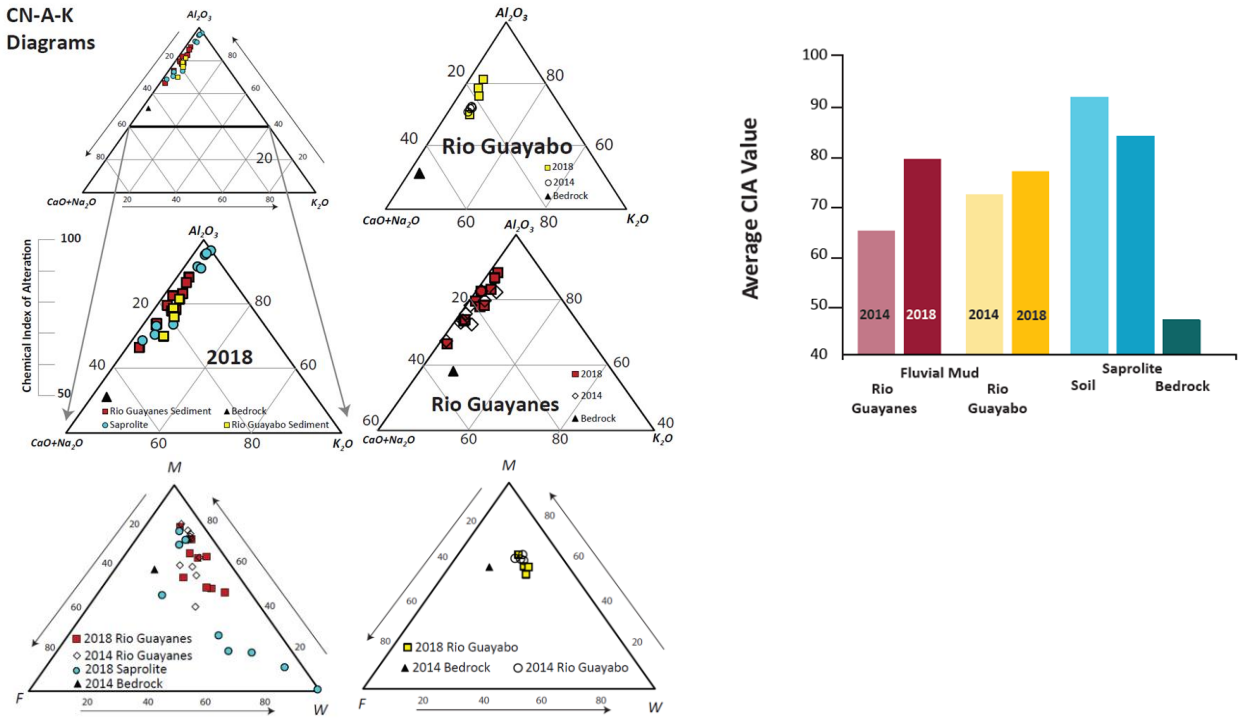

Figure 3: The chemical index of alteration for all samples. All of the samples collected in 2018 are shown on the left. Rio Guayanés sediment (red squares) and saprolite samples (blue circles), Rio Guayabo sediment (yellow squares), bedrock (black triangle). The MFW plot of sediments sampled from hillslopes and bar deposits of Rio Guayanés River (A) and Rio Guayabo River (B) in 2014 (pre-hurricane) and 2018 (post-hurricane). Note: the 2018 fluvial sediments are relatively weathered then that of the 2014 bar sediments. The average values of the chemical index of alteration for all sediment, soil, saprolite, and bedrock samples.

4.3 Rio Guayabo Sediment

The surface area (13.74 - 15.97 m^2/g) in the 2018 Rio Guayabo sediment illustrates very little variability among the four sampling locations (Table 5 in Supplementary Materials). In the 2014 samples, there is higher surface area in the proximal samples (24.64 - 32.05 m^2/g) and then the surface area decreases distally (15.41 - 15.74 m^2/g), reaching values similar to those observed throughout the 2018 samples (13.74 - 15.97 m^2/g).

The average CIA value of the 2018 Rio Guayabo sediment is 76 (ranging from 70-81) while the 2014 sediment average is slightly lower at 73 (Figure 3). Both these values plot in the middle of the range of values observed in the Rio Guayanés sediment samples (Figure 3). The Rio Guayabo MFW plot (Figure 3, E&F) also indicates more weathered sediment in 2018 compared to 2014. Trends in specific surface area with CIA (as specific surface area increase so did CIA) were very similar for both the 2018 and 2014 samples (Table 6 in Supplementary Materials).

4.4 Saprolite

The grain size distributions and specific surface area of the mud-sized fractions observed in the saprolite samples collected within the watershed are highly variable. The mud size fraction of the saprolite samples consist mainly of clay minerals followed by plagioclase (Table 6 in Supplementary Materials). No systematic trends in mineralogy are observed within the saprolite dataset. The saprolite samples have an average CIA value of 84, ranging from 69-97 (Figure 3 and 5), greater than the average values observed in the fluvial sediment samples from both Rio Guayabo and Rio Guayanés (Figure 3). As the surface area of the saprolite sediment increases, a subsequent increase in the CIA value is also expected; this correlation is strongly observed within the saprolite samples (Table 6 in Supplementary Materials). The saprolite sediment MFW

plot (Figure 3, E & F) also indicates the saprolite samples are significantly more weathered than the fluvial sediments.

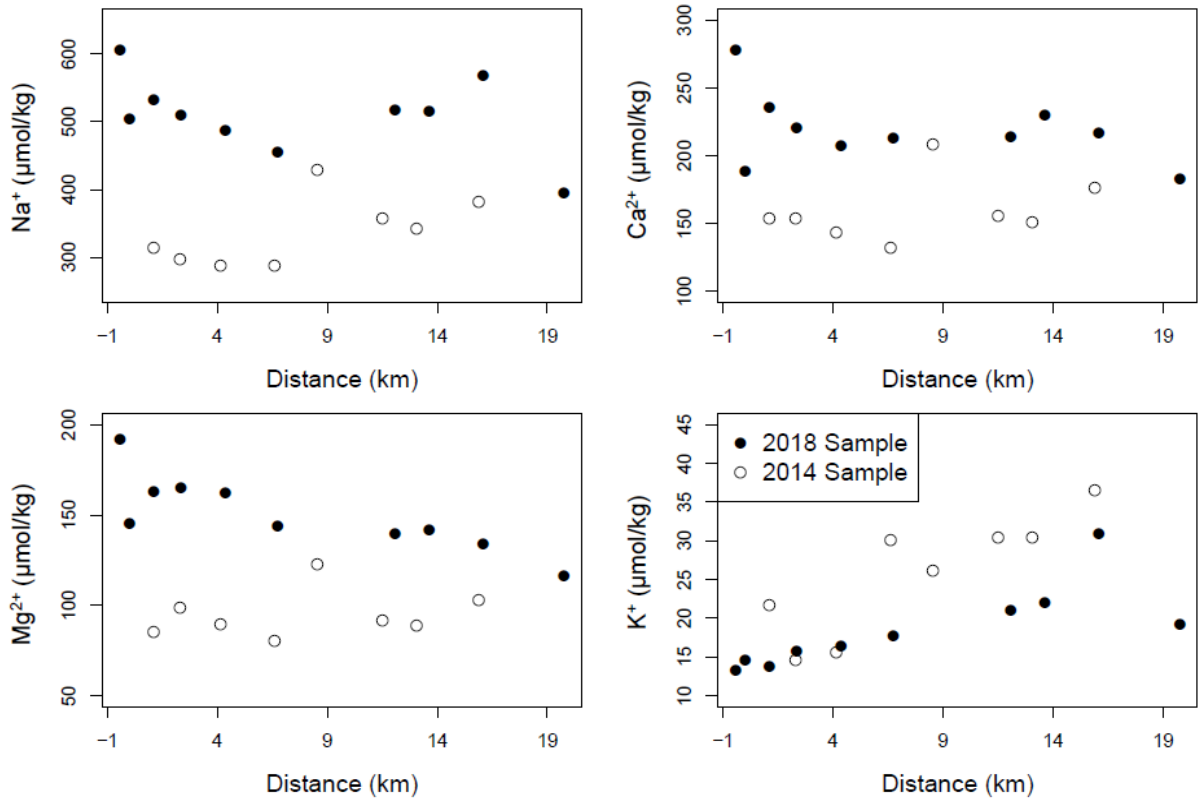

Figure 4. Rio Guayanés stream water chemistry cation concentrations. Na^+, Ca^{2+}, and Mg^{2+} show a general decrease in concentration until approximately 12 km and K^+ shows a general increase distally in 2018. Mg^{2+} and Ca^{2+} show very similar trends to one another while Na^+ is enriched compared to Mg^{2+} and Ca^{2+} but also shows a similar trend.

4.5 Water Chemistry

The 2018 stream water samples had much higher concentrations of Na^+, Ca^{2+}, and Mg^{2+} and lower overall concentration in K^+ compared to the stream water in 2014 (Figure 4). In 2018, the Na^+, Ca^{2+}, and Mg^{2+} concentrations generally decreased from proximal to distal until approximately 12 km where an increase and then subsequent decrease occurs (Figure 4). In the 2014 stream water samples Ca^{2+} and Mg^{2+} have very similar concentrations and follow similar

trends, while Na^+ was consistently enriched relative to the solutes in 2018. K^+ concentrations increased from proximal to distal across the full distance sampled in 2018 (Figure 4).

5. Discussion

As expected, a significant number of landslides occurred within the nine months following Hurricane Maria. This is significantly higher than the background rate of landslides in Puerto Rico (Larsen & Parks, 1997). The prevalence of landslides during this time likely reflects the heavy storm precipitation, in addition to continued anthropogenic forcings, such as deforestation (Larsen & Parks, 1997; Murphy et al., 2012; Silva-Tulla et al., 2020). Additionally, SSURGO soil texture data (U.S. Department of Agriculture, 2019) shows predominant hillslopes are covered by weathered bedrock (mostly granodiorite) and silty clay soil which contains organic materials. These characteristics of soil can facilitate the rapid increase in pore-water pressure during a rainstorm event (C Lepore, Arnone, Noto, Sivandran, & Bras, 2013) and predispose hillslopes to landslides. We initially hypothesized that hurricane-induced landslides would sample the deeper bedrock (Joo et al., 2018). However, despite receiving half a meter of rainfall within four days, our results indicate that the Hurricane Maria-induced landslides are dominated by shallow and small-sized landslides that moved mostly shallow slope materials, including weathered topsoil and saprolite, and only a small amount of less-weathered bedrock (Table 7 in Supplementary Materials). This model is well supported by all our results, including landslide mapping, as well as the weathering index values and MFW plots for the post-hurricane fluvial samples which were higher than those observed in pre-hurricane samples (Figure 3). However, some of the larger landslides that occurred in steeper slopes could have transported deeper soil and less-weathered bedrock, but the volume of the transported materials was likely

small compared to the total volume transported by all landslides (Figure 2). Even larger or more sustained precipitation events may be more likely to produced deeper landslides.

We also expected the fluvial sediment grain size would increase post Hurricane Maria due to the delivery of less-weathered sediments to the stream via landslides. Instead, most of the samples from Rio Guayanés show decreased weight percent of gravel and increased weight percent of sand, mud, and silt size fractions in 2018 versus in 2014 (Figure 8 in Supplementary Materials). However, the pattern is more complicated if we consider the particle size mode (Struck et al., 2015) of the mud fraction, which indicates coarser-grained mud size fraction sediments were delivered to the fluvial system upstream [sample locations 1-4], a decrease mid-stream [sample locations 5-6], followed by an increase downstream [sample locations 7-10] (Figure 1). This indicates that relatively coarser mud was delivered to the Rio Guayanés fluvial system in 2018, despite the overall finer grain size trend observed in the bulk sediment.

If landslides are the dominant source of sediment to the streams, we would not expect to see a trend in mineralogy as we moved downstream, but instead we would expect to see constant or variable mineralogy related to distance. Indeed, the mineralogy results from the x-ray diffraction data indicate no systematic trend in mineralogy within the mud-sized fraction from proximal to distal (Table 3 in Supplementary Materials). Since we observed no systematic trend downstream in both particle mode and mineralogy this indicates little sorting within the fluvial system, nor is there a significant change in the sediment source from proximal to distal stretches of the steam.

Results from the aqueous cation concentrations in the stream were similar to the results obtained by Joo et al. (2018) in that the Na^{+}, Ca^{2+}, and Mg^{2+} generally decreased distally while the K^{+} increased (Figure 4). However, the overall concentration of the solutes in 2018 was

389 greater than in 2014 for every cation with the exception of K^+ (Figure 4). This suggests that
390 landslides impact fluvial systems by delivering both solutes and sediments to streams. Increased
391 cation concentrations may lead to eventual carbonate precipitation downstream following a mass
392 wasting event, resulting in a net carbon sink (Joo et al., 2018).

393 The anomalously low CIA values observed in the fluvial sediments collected before
394 Hurricane Maria (Figures 3 and 5) (Joo et al., 2018) were previously interpreted as deriving from
395 deep seated landslides that delivered partially weathered regolith to the fluvial systems. These
396 deeper seated landslides could be a result of tectonics (Bessette-Kirton et al., 2019; Masson &
397 Scanlon, 1991; Reid & Taber, 1920) and/or anthropogenic forcing such as the construction of
398 roads in the hillsides (Larsen & Parks, 1997; Murphy et al., 2012). In addition, there may also be
399 a time dependent sediment accumulation / depletion effect. For example, the fluvial sediments
400 collected in 2014 may be the accumulated results of deposits from large landslides over a longer
401 period of time, whereas this study reports the response of a rapid flux of sediment from very
402 shallow landslides triggered by a short duration, but intense rainfall. The last severe weather
403 event in Puerto Rico prior to 2014 was Hurricane Irene of 2011. It is possible that streams may
404 have removed much of the sediments delivered by Irene-induced shallow landslides by 2014, and
405 the 2014 observations of Joo et al. are indicating longer-term sediment properties. While the
406 overall transport mechanism is essentially the same, variations in the initial cause of the mass
407 wasting and the duration of sediment transport between the events likely differ. In either case,
408 the change in weathering index values observed in the sediment record are not indicative of the
409 rate of climate change (Figure 5) but are instead a reflection of the stochastic nature of mass
410 wasting.

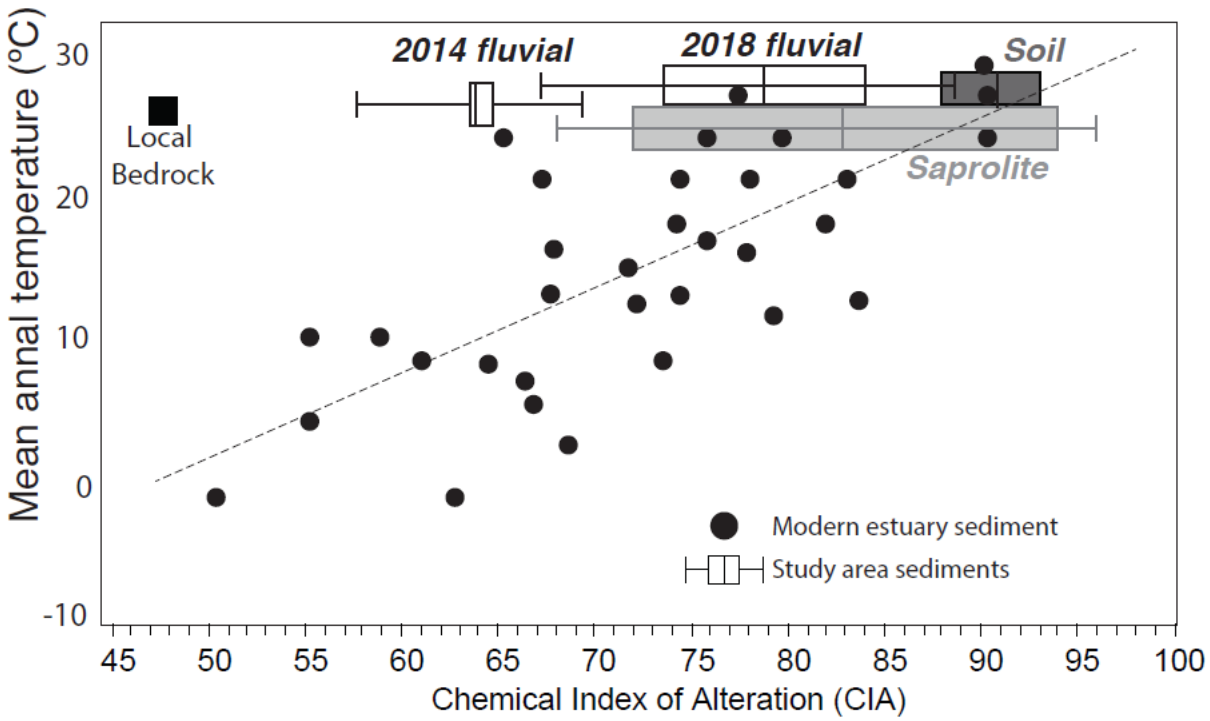

411

412 Figure 5. Plot from Joo et al. demonstrating the linear relationship between chemical index of
413 alteration and mean annual temperatures. 2018 linear relationship of saprolite values plotted as
414 light gray box, sediment range of values indicated with white box, and soil range indicated as
415 dark gray box.

416 **6. Conclusions and Implications**

417 While the initial disturbance of mass wasting events can trigger carbon release to the
418 atmosphere through perturbation of the short-term carbon cycle (e.g. destruction of vegetation), a
419 longer-term result is increased silicate weathering leading to drawdown of atmospheric carbon
420 (Fisk et al., 2013; Hall et al., 2020). The exposure of fresh bedrock through mechanical
421 weathering due to landslides accentuates chemical weathering as water is allowed to interact
422 with fresh bedrock (Oliva et al., 2003). Fresh surfaces lack weathered rindlets (Turner, Stallard,
423 & Brantley, 2003), soils, or clay, enhancing susceptibility to chemical weathering (White et al.,
424 1998). Likewise, the sediment released by landslides can be stored on hillslopes or delivered to
425 fluvial systems (Clark et al., 2016; Hilton, Meunier, Hovius, Bellingham, & Galy, 2011).

Deposition of the material on hillslopes can result in longer-term carbon sequestration due to chemical weathering of the transported material (Clark et al., 2016; Fisk et al., 2013; Hall et al., 2020; Hilton et al., 2011; Ramos Scharrón, Castellanos, & Restrepo, 2012). Sediments entering fluvial systems tend to have a more variable and unconstrained outcome in regards to carbon sequestration amounts (Clark et al., 2016; Ramos Scharrón et al., 2012) but deposition of carbonates that consume cations released via chemical weathering results in a long-term net carbon sink. The landslide scarps sequester carbon over periods of tens to hundreds of years as forest recovery sequesters more carbon in both plants and soils compared to mature forests (Fisk et al., 2013; Hall et al., 2020; Hilton et al., 2011). Our data also demonstrate that even relatively small landslides can increase cation fluxes into stream systems, which deliver cations to the ocean where carbonate minerals likely precipitate, thus further accentuating the carbon sink. Therefore, the magnitude of a storm and associated rainfall accumulation amounts coupled with a variety of variables such as lithology, anthropogenic disturbances, and degree of hillslope can significantly affect carbon sequestration.

In addition, this study also provides high resolution data that shows how the grain size and chemistry of fluvial sediments vary over time in systems that are heavily influenced by mass wasting within the sediment transport system. Our results show hillslope dynamics closely influence fluvial sediment properties and may provide an avenue for interpreting the relative size of landslides based on trends in fluvial sediment observed in close temporal proximity of the triggering event.

Significant differences in the weathering index observed pre- and post- Hurricane Maria are not reflective of the degree of climate change over four years, but rather are indicative of numerous small landslide events that released of large volumes of pre-weathered soil and

saprolite material into the fluvial system. Lower weathering index values observed before the hurricane are likely due to deep-seated landslides caused by tectonics, longer-term groundwater fluctuations, or road building that sampled deeper, less weathered materials including bedrock and regolith. Therefore, this subtle change in the transport mechanism can result in rather large differences in the weathering values recorded by the fluvial system.

These results and their implications can be translated to interpreting chemical weathering indices in different climatic and tectonic environments worldwide, and even on other planets, such as on Mars (e.g., Thorpe, Hurowitz, & Siebach, 2021), particularly when analyzing fluvial or lowland sediments within impact craters. Impact craters have a significant portion of sediment delivered to the floor via mass wasting along the crater walls. Tectonics on Mars likely results in large landslides (e.g., Lamb, Howard, Dietrich, & Perron, 2007; Lucas & Mangeney, 2007) and can be expected that subtle changes in the size of landslides can have significant impact on the weathering index values observed in landslide-derived fluvial sediments, independent of climate.

6. Acknowledgments

Funding was provided by the National Science Foundation grant EAR-1543344. We thank the University of Oklahoma for funding publication costs. Additional data available in the Supplementary Materials.

References

Aristizábal, E., Roser, B., & Yokota, S. (2005). Tropical chemical weathering of hillslope deposits and bedrock source in the Aburrá Valley, northern Colombian Andes. *Engineering Geology, 81*(4), 389-406.

Attal, M., Mudd, S., Hurst, M., Weinman, B., Yoo, K., & Naylor, M. (2015). Impact of change in erosion rate and landscape steepness on hillslope and fluvial sediments grain size in the Feather River basin (Sierra Nevada, California). *Earth Surface Dynamics, 3*(1), 201-222.

Babechuk, M., Widdowson, M., & Kamber, B. (2014). Quantifying chemical weathering intensity and trace element release from two contrasting basalt profiles, Deccan Traps, India. *Chemical Geology, 363*, 56-75.

476 Berner, R. A. (2003). The long-term carbon cycle, fossil fuels and atmospheric composition.
477 *Nature*, *426*(6964), 323-326.
478 Bessette-Kirton, E. K., Cerovski-Darriau, C., Schulz, W. H., Coe, J. A., Kean, J. W., Godt, J. W.,
479 . . . Hughes, K. S. (2019). Landslides triggered by Hurricane Maria: Assessment of an
480 extreme event in Puerto Rico. *GSA Today*, *29*(6), 4-10.
481 Birdsey, R. A., & Weaver, P. L. (1982). The forest resources of Puerto Rico. *Resour. Bull. SO-*
482 *85. New Orleans, Louisiana: US Department of Agriculture, Forest Service, Southern*
483 *Forest Experiment Station. 65 p., 85*.
484 Bluth, G. J., & Kump, L. R. (1994). Lithologic and climatologic controls of river chemistry.
485 *Geochimica et Cosmochimica Acta*, *58*(10), 2341-2359.
486 Brunauer, S., Emmett, P. H., & Teller, E. (1938). Adsorption of gases in multimolecular layers.
487 *Journal of the American chemical society*, *60*(2), 309-319.
488 Clark, K. E., West, A. J., Hilton, R. G., Asner, G. P., Quesada, C. A., Silman, M. R., . . .
489 Horwath, A. B. (2016). Storm-triggered landslides in the Peruvian Andes and
490 implications for topography, carbon cycles, and biodiversity. *Earth Surface Dynamics*,
491 *4*(1), 47-70.
492 Clarke, B. A., & Burbank, D. W. (2011). Quantifying bedrock-fracture patterns within the
493 shallow subsurface: Implications for rock mass strength, bedrock landslides, and
494 erodibility. *Journal of Geophysical Research: Earth Surface*, *116*(F4).
495 Dixon, J. L., Heimsath, A. M., Kaste, J., & Amundson, R. (2009). Climate-driven processes of
496 hillslope weathering. *Geology*, *37*(11), 975-978.
497 Emberson, R., Galy, A., & Hovius, N. (2018). Weathering of reactive mineral phases in
498 landslides acts as a source of carbon dioxide in mountain belts. *Journal of Geophysical*
499 *Research: Earth Surface*, *123*(10), 2695-2713.
500 Fernandes, A. M., da Conceição, F. T., Junior, E. P. S., de Souza Sardinha, D., & Mortatti, J.
501 (2016). Chemical weathering rates and atmospheric/soil CO2 consumption of igneous
502 and metamorphic rocks under tropical climate in southeastern Brazil. *Chemical Geology*,
503 *443*, 54-66.
504 Fisk, J., Hurtt, G., Chambers, J., Zeng, H., Dolan, K., & Negrón-Juárez, R. (2013). The impacts
505 of tropical cyclones on the net carbon balance of eastern US forests (1851–2000).
506 *Environmental Research Letters*, *8*(4), 045017.
507 Fletcher, R., Buss, H. L., & Brantley, S. L. (2006). A spheroidal weathering model coupling
508 porewater chemistry to soil thicknesses during steady-state denudation. *Earth and*
509 *Planetary Science Letters*, *244*(1-2), 444-457.
510 Gariano, S. L., & Guzzetti, F. (2016). Landslides in a changing climate. *Earth-Science Reviews*,
511 *162*, 227-252.
512 Goldberg, K., & Humayun, M. (2010). The applicability of the Chemical Index of Alteration as a
513 paleoclimatic indicator: An example from the Permian of the Paraná Basin, Brazil.
514 *Palaeogeography, Palaeoclimatology, Palaeoecology*, *293*(1-2), 175-183.
515 Guzzetti, F., Ardizzone, F., Cardinali, M., Galli, M., Reichenbach, P., & Rossi, M. (2008).
516 Distribution of landslides in the Upper Tiber River basin, central Italy. *Geomorphology*,
517 *96*(1-2), 105-122.
518 Hall, J., Muscarella, R., Quebbeman, A., Arellano, G., Thompson, J., Zimmerman, J. K., &
519 Uriarte, M. (2020). Hurricane-induced rainfall is a stronger predictor of tropical forest
520 damage in Puerto Rico than maximum wind speeds. *Scientific reports*, *10*(1), 1-10.

Harris, W., & Norman White, G. (2008). X-ray diffraction techniques for soil mineral identification. *Methods of soil analysis part 5—Mineralogical methods, 5*, 81-115.

Hilton, R. G., Meunier, P., Hovius, N., Bellingham, P. J., & Galy, A. (2011). Landslide impact on organic carbon cycling in a temperate montane forest. *Earth Surface Processes and Landforms, 36*(12), 1670-1679.

Hubert, J. F., & Filipov, A. J. (1989). Debris-flow deposits in alluvial fans on the west flank of the White Mountains, Owens Valley, California, USA. *Sedimentary Geology, 61*(3-4), 177-205.

Joo, Y. J., Elwood Madden, M. E., & Soreghan, G. S. (2018). Anomalously low chemical weathering in fluvial sediment of a tropical watershed (Puerto Rico). *Geology, 46*(8), 691-694.

Keellings, D., & Ayala, J. J. H. (2019). Extreme rainfall associated with Hurricane Maria over Puerto Rico and its connections to climate variability and change. *Geophysical research letters, 46*(5), 2964-2973.

Lamb, M. P., Howard, A. D., Dietrich, W. E., & Perron, J. T. (2007). Formation of amphitheater-headed valleys by waterfall erosion after large-scale slumping on Hawai 'i. *Geological Society of America Bulletin, 119*(7-8), 805-822.

Larsen, M. C. (2000). Analysis of 20th century rainfall and streamflow to characterize drought and water resources in Puerto Rico. *Physical Geography, 21*(6), 494-521.

Larsen, M. C., & Parks, J. E. (1997). How wide is a road? The association of roads and mass-wasting in a forested montane environment. *Earth Surface Processes and Landforms: The Journal of the British Geomorphological Group, 22*(9), 835-848.

Larsen, M. C., & Torres-Sanchez, A. J. (1998). The frequency and distribution of recent landslides in three montane tropical regions of Puerto Rico. *Geomorphology, 24*(4), 309-331.

Lehmann, P., Gambazzi, F., Suski, B., Baron, L., Askarinejad, A., Springman, S. M., . . . Or, D. (2013). Evolution of soil wetting patterns preceding a hydrologically induced landslide inferred from electrical resistivity survey and point measurements of volumetric water content and pore water pressure. *Water Resources Research, 49*(12), 7992-8004.

Lepore, C., Arnone, E., Noto, L., Sivandran, G., & Bras, R. L. (2013). Physically based modeling of rainfall-triggered landslides: a case study in the Luquillo forest, Puerto Rico. *Hydrology and Earth System Sciences, 17*(9), 3371-3387.

Lepore, C., Kamal, S. A., Shanahan, P., & Bras, R. L. (2012). Rainfall-induced landslide susceptibility zonation of Puerto Rico. *Environmental Earth Sciences, 66*(6), 1667-1681.

Lucas, A., & Mangeney, A. (2007). Mobility and topographic effects for large Valles Marineris landslides on Mars. *Geophysical research letters, 34*(10).

Martinuzzi, S., Gould, W. A., & González, O. M. R. (2007). Land development, land use, and urban sprawl in Puerto Rico integrating remote sensing and population census data. *Landscape and urban planning, 79*(3-4), 288-297.

Masson, D., & Scanlon, K. M. (1991). The neotectonic setting of Puerto Rico. *Geological Society of America Bulletin, 103*(1), 144-154.

Monroe, W. H. (1980). *Geology of the middle Tertiary formations of Puerto Rico*: US Government Printing Office.

Moore, O. W., Buss, H. L., & Dosseto, A. (2019). Incipient chemical weathering at bedrock fracture interfaces in a tropical critical zone system, Puerto Rico. *Geochimica et Cosmochimica Acta, 252*, 61-87.

Murphy, S. F., Stallard, R. F., Larsen, M. C., & Gould, W. A. (2012). Physiography, geology, and land cover of four watersheds in eastern Puerto Rico. *Professional Paper 1789-A. Reston, VA (?): US Department of the Interior, US Geological Survey.*

Nesbitt, H., & Young, G. (1982). Early Proterozoic climates and plate motions inferred from major element chemistry of lutites. *Nature, 299*(5885), 715-717.

Ohta, T., & Arai, H. (2007). Statistical empirical index of chemical weathering in igneous rocks: A new tool for evaluating the degree of weathering. *Chemical Geology, 240*(3-4), 280-297.

Oliva, P., Viers, J., & Dupré, B. (2003). Chemical weathering in granitic environments. *Chemical Geology, 202*(3-4), 225-256.

Phillips, J. D., Marion, D. A., Luckow, K., & Adams, K. R. (2005). Nonequilibrium regolith thickness in the Ouachita Mountains. *The Journal of geology, 113*(3), 325-340.

Ramos-Scharrón, C. E., & Arima, E. (2019). Hurricane María's precipitation signature in Puerto Rico: A conceivable presage of rains to come. *Scientific reports, 9*(1), 1-7.

Ramos Scharrón, C. E., Castellanos, E. J., & Restrepo, C. (2012). The transfer of modern organic carbon by landslide activity in tropical montane ecosystems. *Journal of Geophysical Research: Biogeosciences, 117*(G3), n/a-n/a. doi:10.1029/2011jg001838

Regmi, N. R., Giardino, J. R., & Vitek, J. D. (2014). Characteristics of landslides in western Colorado, USA. *Landslides, 11*(4), 589-603.

Reid, H. F., & Taber, S. (1920). The Virgin Islands earthquakes of 1867-1868. *Bulletin of the Seismological Society of America, 10*(1), 9-30.

Roda-Boluda, D. C., D'Arcy, M., McDonald, J., & Whittaker, A. C. (2018). Lithological controls on hillslope sediment supply: insights from landslide activity and grain size distributions. *Earth Surface Processes and Landforms, 43*(5), 956-977.

Rogers, C. L., Cram, C., Pease, M., & Tischler, M. (1977). *Geologic map of the Yabucoa and Punta Tuna quadrangles, Puerto Rico* (2331-1258). Retrieved from

Sassa, K., & Canuti, P. (2008). *Landslides-disaster risk reduction*: Springer Science & Business Media.

Schmidt, K. M., & Montgomery, D. R. (1995). Limits to relief. *Science, 270*(5236), 617-620.

Shiels, A. B., & Walker, L. R. (2013). Landslides cause spatial and temporal gradients at multiple scales in the Luquillo Mountains of Puerto Rico. *Ecological Bulletins*(54), 211-222.

Silva-Tulla, F., Pando, M. A., Pradel, D., Park, Y., & Kayen, R. (2020). *Geotechnical Consequences and Failures in Puerto Rico Due to Hurricane Maria.* Paper presented at the Geo-Congress 2020: Engineering, Monitoring, and Management of Geotechnical Infrastructure.

Stark, C. P., & Hovius, N. (2001). The characterization of landslide size distributions. *Geophysical research letters, 28*(6), 1091-1094.

Struck, M., Andermann, C., Hovius, N., Korup, O., Turowski, J. M., Bista, R., . . . Dahal, R. K. (2015). Monsoonal hillslope processes determine grain size-specific suspended sediment fluxes in a trans-Himalayan river. *Geophysical research letters, 42*(7), 2302-2308.

Thorpe, M. T., Hurowitz, J. A., & Siebach, K. L. (2021). Source-to-sink terrestrial analogs for the paleoenvironment of Gale crater, Mars. *Journal of Geophysical Research: Planets, 126*(2), e2020JE006530.

Tron, S., Dani, A., Laio, F., Preti, F., & Ridolfi, L. (2014). Mean root depth estimation at landslide slopes. *Ecological engineering, 69*, 118-125.

Turner, B. F., Stallard, R. F., & Brantley, S. L. (2003). Investigation of in situ weathering of quartz diorite bedrock in the Rio Icacos basin, Luquillo Experimental Forest, Puerto Rico. *Chemical Geology, 202*(3-4), 313-341.

U.S. Department of Agriculture, N. R. C. S. (2019). *Soil Survey Geographic (SSURGO) database for Humacao Area, Puerto Rico Eastern Part*. Fort Worth, Texas: U.S. Department of Agriculture, Natural Resources Conservation Service.

Varnes, D. J. (1978). Slope movement types and processes. *Special report, 176*, 11-33.

White, A. F., & Blum, A. E. (1995). Effects of climate on chemical_ weathering in watersheds. *Geochimica et Cosmochimica Acta, 59*(9), 1729-1747.

White, A. F., Blum, A. E., Schulz, M. S., Bullen, T. D., Harden, J. W., & Peterson, M. L. (1996). Chemical weathering rates of a soil chronosequence on granitic alluvium: I. Quantification of mineralogical and surface area changes and calculation of primary silicate reaction rates. *Geochimica et Cosmochimica Acta, 60*(14), 2533-2550.

White, A. F., Blum, A. E., Schulz, M. S., Vivit, D. V., Stonestrom, D. A., Larsen, M., . . . Eberl, D. (1998). Chemical weathering in a tropical watershed, Luquillo Mountains, Puerto Rico: I. Long-term versus short-term weathering fluxes. *Geochimica et Cosmochimica Acta, 62*(2), 209-226.

White, A. F., Bullen, T. D., Vivit, D. V., Schulz, M. S., & Clow, D. W. (1999). The role of disseminated calcite in the chemical weathering of granitoid rocks. *Geochimica et Cosmochimica Acta, 63*(13-14), 1939-1953.